

# Influence of the STS-78 Space Shuttle Exhaust Plume on Column Ozone Abundance Inferred from Ground-level Solar UV Spectra

15 February 1997

Prepared by

D. L. McKENZIE, D. J. GUTIERREZ, and J. H. HECHT  
Space and Environment Technology Center  
Technology Operations

Prepared for

SPACE AND MISSILE SYSTEMS CENTER  
AIR FORCE MATERIEL COMMAND  
2430 E. El Segundo Boulevard  
Los Angeles Air Force Base, CA 90245

Space Systems Group

APPROVED FOR PUBLIC RELEASE;  
DISTRIBUTION UNLIMITED

DTIC QUALITY INSPECTED 1

19970529 012




**THE AEROSPACE  
CORPORATION**  
El Segundo, California

This report was submitted by The Aerospace Corporation, El Segundo, CA 90245-4691, under Contract No. F04701-93-C-0094 with the Space and Missile Systems Center, 2430 E. El Segundo Blvd., Los Angeles Air Force Base, CA 90245. It was reviewed and approved for The Aerospace Corporation by A. B. Christensen Principal Director, Space and Environment Technology Center. Maj. R. Reiners was the project officer for the program.

This report has been reviewed by the Public Affairs Office (PAS) and is releasable to the National Technical Information Service (NTIS). At NTIS, it will be available to the general public, including foreign nationals.

This technical report has been reviewed and is approved for publication. Publication of this report does not constitute Air Force approval of the report's findings or conclusions. It is published only for the exchange and stimulation of ideas.



Maj. R. Reiners  
SMC/CLNM

REPORT DOCUMENTATION PAGE			Form Approved OMB No. 0704-0188	
Public reporting burden for this collection of information is estimated to average 1 hour per response, including the time for reviewing instructions, searching existing data sources, gathering and maintaining the data needed, and completing and reviewing the collection of information. Send comments regarding this burden estimate or any other aspect of this collection of information, including suggestions for reducing this burden to Washington Headquarters Services, Directorate for Information Operations and Reports, 1215 Jefferson Davis Highway, Suite 1204, Arlington, VA 22202-4302, and to the Office of Management and Budget, Paperwork Reduction Project (0704-0188), Washington, DC 20503.				
1. AGENCY USE ONLY (Leave blank)		2. REPORT DATE 15 February 1997		3. REPORT TYPE AND DATES COVERED
4. TITLE AND SUBTITLE Influence of the STS-78 Space Shuttle Exhaust Plume on Column Ozone Abundance Inferred from Ground-level Solar UV Spectra			5. FUNDING NUMBERS  F04701-93-C-0094	
6. AUTHOR(S) D. L. McKenzie, D. J. Gutierrez, and J. H. Hecht				
7. PERFORMING ORGANIZATION NAME(S) AND ADDRESS(ES) The Aerospace Corporation Technology Operations El Segundo, CA 90245-4691			8. PERFORMING ORGANIZATION REPORT NUMBER  TR-97(1410)-1	
9. SPONSORING/MONITORING AGENCY NAME(S) AND ADDRESS(ES) Space and Missile Systems Center Air Force Materiel Command 2430 E. El Segundo Boulevard Los Angeles Air Force Base, CA 90245			10. SPONSORING/MONITORING AGENCY REPORT NUMBER  SMC-TR-97-06	
11. SUPPLEMENTARY NOTES				
12a. DISTRIBUTION/AVAILABILITY STATEMENT  Approved for public release; distribution unlimited			12b. DISTRIBUTION CODE	
13. ABSTRACT (Maximum 200 words) The ground-based prototype of the High Resolution Ozone Imager (HIROIG), an imaging spectrograph that was operated in the wavelength range 275–360 nm, was deployed at Kennedy Space Center on June 19–21, 1996 to make observations before, during, and after the launch of the STS-78 space shuttle mission. The instrument measured the ultraviolet (UV) spectrum of direct sunlight at the ground every 74 s for several hours during each of the three days. The objective of the campaign was to search for evidence of stratospheric ozone depletion in the launch plume. To accomplish this, we examined, as functions of time, several spectral ratios that are sensitive to the total column ozone abundance along the line of sight to the sun. The spectral ratios yielded no evidence of column ozone depletion caused by the launch plume as it occulted the sun. The upper limit, at the 95% confidence level, on column ozone depletion for the entire 10-min period during which the plume was between the spectrograph and the sun was 3.4%. Since the potential harmful effect of ozone depletion, increased ultraviolet radiation at the ground, may be mitigated by increased scattering or absorption by rocket-plume aerosols, we also examined the absolute intensities at 300.8 and 307.5 nm wavelengths. There was no evidence of significant reduction in UV intensity attributable to the effects of plume aerosols, but the absolute flux measurements were complicated by the intermittent obscuration of the sun by tropospheric clouds. The upper limit on UV attenuation by scattering from plume aerosols is approximately 15% at 300.8 nm.				
14. SUBJECT TERMS  Ozone, Stratosphere, Ozone depletion, Solid-fuel rocket motors, UV spectrograph			15. NUMBER OF PAGES 17	
			16. PRICE CODE	
17. SECURITY CLASSIFICATION OF REPORT UNCLASSIFIED	18. SECURITY CLASSIFICATION OF THIS PAGE UNCLASSIFIED	19. SECURITY CLASSIFICATION OF ABSTRACT UNCLASSIFIED	20. LIMITATION OF ABSTRACT	

## Contents

1. Introduction .....	1
2. Observations .....	3
3. Data Analysis.....	5
3.1 Effects of Total Column Ozone .....	5
3.2 Effects of Aerosols.....	10
4. Conclusions .....	15
References .....	17

## Figures

1. The integrating sphere fitted to the entrance cone of the UV spectrograph used to acquire solar UV spectra on the ground around the STS-78 launch.....	3
2. The ratio $R_1$ of UV intensities at 299.7 and 297.9 nm plotted as a function of time on June 20, 1996, the day of the STS-78 launch .....	6
3. A plot of the ratio $R_2$ of UV intensities at 300.8 and 299.0 nm for June 20, 1996 similar to Figure 2 .....	9
4. Detector counts in a band centered on 300.8 nm plotted as a function of time on June 20, 1996 .....	11
5. Similar to Figure 4 for a band centered on 307.5 nm.....	12
6. $R_1$ plotted as in Figure 2 but for June 19, 1996 .....	13

## 1. Introduction

Solid-fuel rocket motors (SRMs) deposit several tons of chlorine per kilometer in the form of HCl into the atmosphere below their burn-out altitude of approximately 40 km (Ross 1996). Computer simulations and theoretical analysis have suggested that significant amounts of HCl are converted to the active species Cl and Cl<sub>2</sub> by afterburning reactions in the atmosphere (Zittel 1994; Denison, *et al.* 1994). The active-chlorine afterburning products can interact with and consume stratospheric ozone, resulting in creation of a transient stratospheric "ozone hole." This is of concern because the stratospheric ozone layer acts as a shield that absorbs biologically harmful ultraviolet (UV) radiation before it reaches the ground. The Rocket Impacts on Stratospheric Ozone (RISO) program encompasses a series of ground-based observations and airborne *in-situ* measurements with the goal of assessing the extent of any ozone depletion that might develop following an SRM launch and the net effect of launches on the flux of UV radiation at the ground.

As part of the RISO program the ground-based prototype of the High Resolution Ozone Imager (HIROIG) space instrument was deployed at Kennedy Space Center to make direct-absorption measurements of solar UV radiation around the time of the STS-78 launch. HIROIG is an imaging UV spectrograph; but on this occasion, the imaging capability was not used. Rather, the entrance aperture of the instrument was fitted with an integrating sphere and pointed directly at the sun, which would be too bright to observe without the sphere. Analysis of changes in the UV spectrum with time would allow the detection of any transient ozone depletion region, and measurements of the time variation of the absolute intensity of the radiation would allow an assessment of any increased absorption by launch-plume aerosols. This report presents the results of the STS-78 observing campaign.

## 2. Observations

Hecht, *et al.* (1994) describe the HIROIG instrument in detail. Briefly, it is a novel imaging spectrograph based on the Broadband Array Spectrograph System (Hackwell and Warren 1992) that uses a specially designed prism for its dispersing element. Incident light passes through a window that is opaque in the visible part of the spectrum, a UV attenuator that shapes the spectrum by strongly attenuating radiation at wavelengths longer than 310 nm, a half-wave plate, and a polarizing prism. A three-element telescope focuses the light on the spectrograph entrance slit. The spectrum is imaged onto a charge-coupled device (CCD) detector, with spatial resolution in one direction and the spectrum dispersed in the other. For the STS-78 observations, the spectral range 275–360 nm was detected in 435 detector pixels.

The UV spectrograph was deployed at Cape Canaveral in an observing mode that allowed us to make direct observations of the sun. This required that a collimator followed by an integrating sphere be fitted to the entrance cone of the spectrograph, as shown in Figure 1. The forward collimator was flat

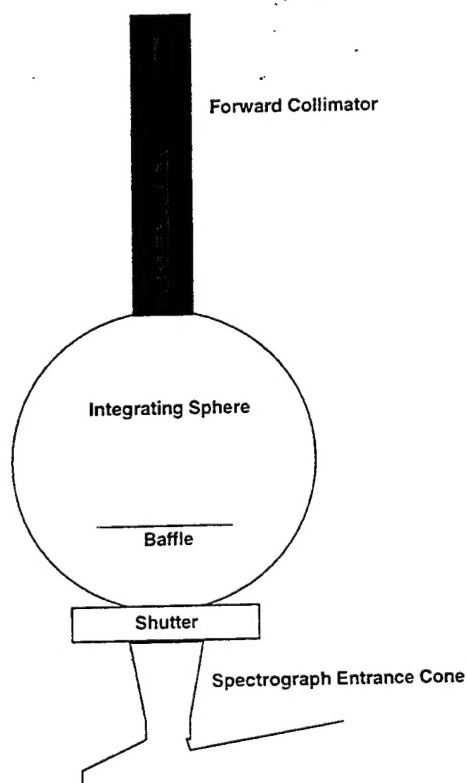


Figure 1. The integrating sphere fitted to the entrance cone of the UV spectrograph used to acquire solar UV spectra on the ground around the STS-78 launch

black. The internal surfaces and the internal baffle in the integrating sphere were all white diffuse reflectors. From the figure, it can be seen that incident solar radiation had to undergo several diffuse reflections inside the integrating sphere before it could enter the spectrograph. These reflections destroyed any imaging information and any polarization (we expect none) of the incident radiation. The polarizing prism in front of the spectrograph reduced the intensity of the incident light by a factor of 2. Although the imaging information was lost, the data were still coarsely binned in the spatial direction into 40 bins that covered approximately 80% of the active area of the detector. In the final data analysis, 31 of these bins were added together to give a single spectrum with the spatial resolution of the instrument determined solely by the forward collimator. Despite all this binning, the signals were relatively weak, and numerous spectra were discarded because tropospheric clouds obscured the sun.

The spectrograph was mounted on a Meade telescope mount that tracked the sun under computer control. The shutter was opened to take a 20-s exposure of the solar spectrum. This was followed by a 20-s dark exposure with the shutter closed. The dark spectrum was subtracted from the solar spectrum in the data analysis. The macro that controlled the exposure also subtracted the dark spectrum from the solar spectrum and stored the result. A pause time was built into each cycle to allow for a quick look at the data. This sequence was repeated continually during the observing hours, with each cycle taking 74 s. The observing hours (Eastern Daylight Time) for the three days were: June 19, 10:00:58–13:29:16; June 20, 07:53:19–13:30:40; and June 21, 09:18:57–12:08:16. On the first two days, the observations were carried out until just past local noon (13:24 EDT), and on June 21 they were terminated because of a sudden thunderstorm.

The STS-78 launch occurred at 10:49 EDT on June 20. Winds in the lower stratosphere blew an isolated plume segment westward such that it lay between the sun and the observing location from 11:03 to 11:14 EDT. Between 11:06 and 11:07, the sun was obscured by a tropospheric cloud. Five exposures taken while the plume was between the sun and the observing site were of sufficient quality to be useful in the data analysis.

### 3. Data Analysis

#### 3.1 Effects of Total Column Ozone

Absorption of UV radiation by ozone varies rapidly with wavelength in the 300 nm range, with stronger absorption at shorter wavelengths. The transmission is

$$T_{O_3}(\lambda) = \exp(-\tau_{O_3}(\lambda)), \quad (1)$$

where the optical depth of the ozone layer is given as a function of wavelength and location along the incident light path by

$$\tau_{O_3}(\lambda) = \int \sigma_{O_3}(\lambda) n_{O_3}(\vec{s}) d\vec{s}. \quad (2)$$

The integrand is the product of the ozone absorption cross section ( $\text{cm}^2$ ) and the ozone density ( $\text{cm}^{-3}$ ). We take advantage of the rapid variation in the ozone absorption cross section with wavelength by looking at the ratio of the UV signal strengths in two closely spaced wavelength bands. Using closely spaced bands assures that effects other than ozone absorption are minimized. Thus, we observe the ratio

$$R_1 = \frac{S(299.7)}{S(297.9)} = \frac{r_1(299.7)I_s(299.7)}{r_1(297.9)I_s(297.9)} \exp(\tau_{O_3}(297.9) - \tau_{O_3}(299.7)) \quad (3)$$

for several hours and search for deviations from the long-term trend that would be indicative of a transient decrease in the ozone density integrated along the line of sight from the sensor to the sun. In Eq. (3)  $r_1$  denotes the instrument response function, and  $I_s$  is the intensity of the solar radiation incident upon the atmosphere. Since the optical path through the atmosphere to the sun is a minimum at local noon when the solar zenith angle is a minimum, we expect  $R_1$  to decrease in the morning and then increase in the afternoon. If the total column ozone is constant or slowly varying, a plot of  $R_1$  as a function of time should be smooth. If there is an abrupt decrease in stratospheric ozone, the ratio will drop abruptly below the smooth curve. Thus, we seek an abrupt decrease in  $R_1$  as evidence of sudden ozone depletion.

Figure 2 is a plot of  $R_1$  as a function of time on June 20, 1996, the day of the STS-78 launch. The smooth curve was derived from a linear minimum-chi-squared fit of the form

$$\ln(R_1) = a + b \sec(\zeta_S(t)), \quad (4)$$



where “ln” denotes the natural logarithm, and  $\zeta_S(t)$  is the solar zenith angle as a function of time [see Eq. (9), below]. The June 20 observations were cut short by threatening weather at 13:31 EDT, which is only a few minutes past local noon, so the expected afternoon increase in  $R_1$  was not observed. The data with the largest error bars correspond to times when clouds obscured the sun. In addition, there were many data samples for which the clouds blocked the sun to such an extent that a usable signal was not obtained; these, of course, are not plotted.

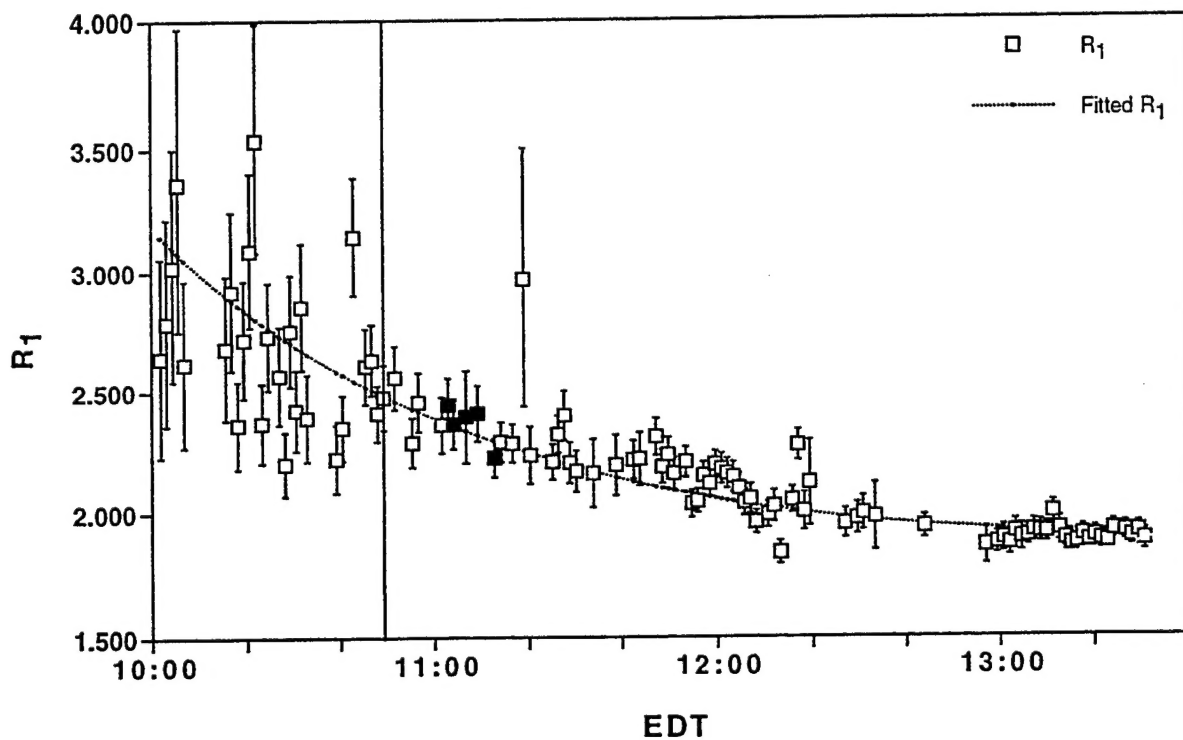


Figure 2. The ratio  $R_1$  of UV intensities at 299.7 and 297.9 nm plotted as a function of time on June 20, 1996, the day of the STS-78 launch. The time of launch, 10:49 EDT is indicated by the vertical line, and the points taken while the plume occulted the sun are shaded. The fitted curve is described in the text.

The stratospheric portion of the STS-78 plume was easily visible and, because lower stratospheric winds generally blew westward and the tropospheric winds generally eastward, it was clearly identified as stratospheric. The plume was observed to pass between the HIROIG site and the sun during the period 11:03–11:13 EDT. Five determinations of  $R_1$  during this period are indicated by shading in Figure 2. There is no evidence of a sharp dip in the ratio that might be indicative of ozone depletion in the plume.

We now calculate an upper limit on the fractional ozone depletion that is consistent with the data at the 95% confidence level. Assume that each of the five determinations of  $R_1$  fall below the fitted curve by  $\delta$ . We will find the maximum value of  $\delta$  that would be consistent with the data. That is,

$$\delta = \frac{\sum_{n=1}^5 R_{1n}(\text{fit})}{5} - \frac{\sum_{n=1}^5 R_{1n}}{5} \quad (5)$$

where

$$\delta = 1.65\sigma_{\text{Ave}} = 1.65 \frac{\sqrt{\sum_{n=1}^5 \sigma_n^2}}{5} \quad (6)$$

The multiplier 1.65 arises from the normal distribution; only 5% of normally distributed data are greater than the mean plus  $1.65\sigma$ . Using *a priori* values of the standard deviation, which are based on counting statistics, we find  $\delta/\langle R_1 \rangle = 0.0401$ . But the *a priori* standard deviations underestimate the variability of the data. The best-fit curve in Figure 2 had a  $\chi^2$  of 170 with 100 degrees of freedom when the *a priori* values were used, an unacceptable fit. Therefore, we scale up the standard deviation by the factor

$$\sqrt{\frac{\chi^2}{N_{\text{dof}}}} = \sqrt{1.70} = 1.31 \quad (7)$$

to obtain

$$\frac{\delta}{\langle R_1 \rangle} = 0.0524 \quad (8)$$

Variations of  $R_1$  are assumed to derive from variations in the total column ozone density. If the total column ozone decreases by a fraction  $\alpha$ , then the optical depth at each wavelength also decreases by this factor. Thus:

$$R_1 \times (1 - \delta) = \frac{r_i(299.7)I_S(299.7)}{r_i(297.9)I_S(297.9)} \exp\left[\left(\tau_{O_3,0}(297.9) - \tau_{O_3,0}(299.7)\right)(1 - \alpha) \sec(\zeta_S)\right], \quad (9)$$

where the subscript 0 indicates the value for normal incidence on the atmosphere ( $\zeta_S = 0$ ). Substituting for  $R_1$  from Eq. (3) and using the ozone absorption coefficients finally gives

$$|\alpha| = \frac{-\ln(1 - \delta) \cos(\zeta_S)}{\left(\tau_{O_3,0}(297.9) - \tau_{O_3,0}(299.7)\right)} < 0.045, \quad (10)$$

for  $\zeta_S = 31.2^\circ$  and a typical average ambient column ozone density of 300 Dobson units. Thus, we derive a 95%-confidence-level upper limit on the average total column ozone depletion of 4.5% for the entire interval during which the stratospheric plume stood between the sun and the viewing site.

The measured spectra had a practical wavelength range of approximately 292–360 nm. In addition to  $R_1$ , a second wavelength ratio,  $R_2$ , was also used to derive an upper limit on the total column ozone depletion during the time that the plume stood between the viewing site and the sun:

$$R_2 = \frac{S(300.8)}{S(299.0)} = \frac{r_i(300.8)I_S(300.8)}{r_i(299.0)I_S(299.0)} \exp\left(\tau_{O_3}(299.0) - \tau_{O_3}(300.8)\right) \quad (11)$$

Figure 3 is a plot of  $R_2$  as a function of time with a fitted curve of the same type as that displayed for  $R_1$ . As with Figure 2, Figure 3 gives no evidence of a decrease in total column ozone during the time that the plume occulted the sun. The counting rates at the longer wavelengths are higher, resulting in smaller *a priori* error bars, but we will see that the scatter in the two plots is similar. Using the *a priori* error bars, we find that  $d/\langle R_1 \rangle = 0.0226$ . The best-fit curve had a  $\chi^2$  of 409.6 with 102 degrees of freedom. Thus, the scaling factor is

$$\sqrt{\frac{\chi^2}{N_{\text{dof}}}} = \sqrt{4.02} = 2.00, \quad (12)$$

and we obtain

$$\frac{\delta}{\langle R_1 \rangle} = 0.0452. \quad (13)$$

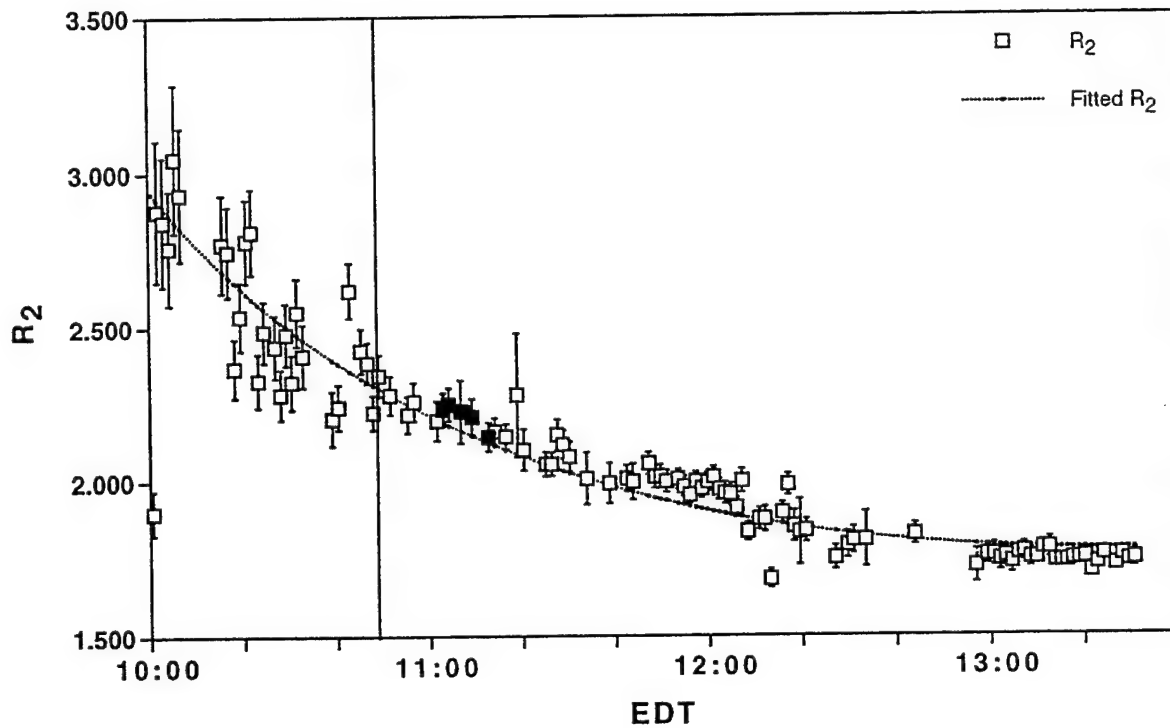


Figure 3. A plot of the ratio  $R_2$  of UV intensities at 300.8 and 299.0 nm for June 20, 1996 similar to Figure 2

Converting this to a 95%-confidence-level upper limit on column ozone depletion, as before, gives

$$|\alpha| = \frac{-\ln(1-\delta)\cos(\zeta_S)}{(\tau_{O_3,0}(299.0) - \tau_{O_3,0}(300.8))} < 0.050 \quad , \quad (14)$$

The upper limit on the average total column ozone depletion for the entire interval during which the stratospheric plume stood between the sun and the viewing site is 5.0%. The results for ratios  $R_1$  and  $R_2$  can be combined to give a final value of 3.4% for the upper limit on total column ozone depletion:

$$|\alpha| < 0.034 \quad . \quad (15)$$

This result is generally consistent with other RISO plume measurements. Burke (1996) used commercial meters to measure the intensity of solar UV light in the UV-A (295–320 nm) and UV-B (320–370 nm) regions of the spectrum during the time stratospheric plumes from a Space Shuttle and Titan-IV launch occulted the sun. No ozone loss was detected with a minimum observable reduction of about 9%.

### 3.2 Effects of Aerosols

The potentially harmful increase in solar UV intensity associated with plume ozone depletion might be mitigated by backscattering of the incident UV radiation by the aerosols in the visible plume. In addition, aerosol scattering might mask ozone depletion as determined from ground-based UV spectra. Based on his earlier RISO lidar measurements, Phan Dao has concluded that, during the first approximately 45 min after launch, plume aerosols scatter with a Rayleigh-scattering wavelength dependence (Dao 1997):

$$\sigma_{\text{scatter}} \propto \lambda^{-4}, \quad (16)$$

where  $\sigma_{\text{scatter}}$  is the scattering cross-section and  $\lambda$  is the wavelength of the radiation. Therefore, we can amend Eq. (11) for  $R_2$  to take into account the wavelength-dependent effects of aerosol backscattering of the incident radiation:

$$R_2 \propto \exp(\tau_{O_3}(299.0) - \tau_{O_3}(300.8)) \exp\left(\tau_R(300.8) \left(\left(\frac{300.8}{299.0}\right)^4 - 1\right)\right). \quad (17)$$

The Rayleigh scattering optical depth associated with the plume (*i.e.*, excluding Rayleigh scattering in the ambient atmosphere) is  $\tau_R$ . From the expression, we see that a decrease in ozone along the path between the observer and the sun might be counteracted in its effect on  $R_2$  (or  $R_1$ ) by increased scattering by plume aerosols.

To assess the role that aerosols play in providing protection from UV radiation on the ground and in counteracting any ozone depletion that might occur, we turn to the measured intensities of the UV radiation. This is complicated by the fact that absolute intensities are much more sensitive to tropospheric clouds than are the intensity ratios  $R_1$  and  $R_2$ . Figure 4 is a plot of the detector counts in a wavelength band centered on 300.8 nm. The curve is a fit to a function of the form in Eq. (4), including all of the data up to 12:00 EDT; after that time the data are severely affected by tropospheric clouds. Five points taken during the time of plume passage between the instrument and the sun are shaded. One of these points, at 11:06.8 EDT, deviates far below the fitted curve. A log book notation states that the sun was obscured by a tropospheric cloud at this time. It is interesting to note that the cloud had no discernible effect on  $R_1$  or  $R_2$ . The spectrum taken immediately after the one at 11:06.8 was so faint as to be unusable. The four other points, for which tropospheric clouds played no role, show no evidence of attenuation of the UV radiation by plume aerosols. Following the method used in Eqs. (6) through (8), we find a 95%-confidence-level upper limit on the decrease in counting rate for the four points not affected by tropospheric clouds:

$$\frac{\delta_{300.8}}{C_{300.8}} = 0.154. \quad (18)$$

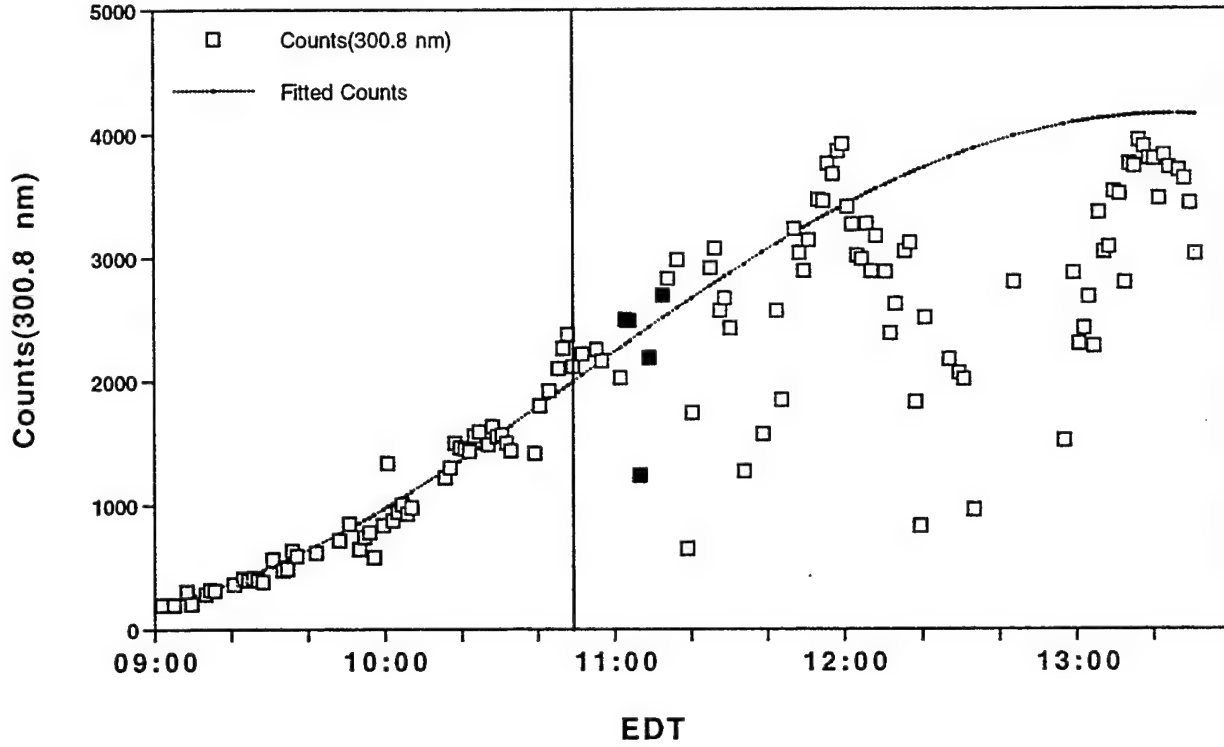


Figure 4. Detector counts in a band centered on 300.8 nm plotted as a function of time on June 20, 1996. The time of the STS-78 launch is marked by the vertical line.

The corresponding upper limit on  $\tau_R(300.8 \text{ nm})$  is given by

$$\tau_R(300.8) < -\ln\left(1 - \frac{\delta_{300.8}}{\langle C_{300.8} \rangle}\right) = 0.167 . \quad (19)$$

The large size of this number results from the large scatter in the data. Much of this was caused by tropospheric clouds. In order to avoid injecting bias, no measured counting rate before 12:00 EDT was eliminated from the fit in Figure 4 no matter how "obvious" the influence of tropospheric clouds.

Figure 5 is the same as Figure 4 but is plotted for a wavelength of 307.5 nm. It is very similar to Figure 4; again there is no evidence for reduced signal strength during the time of plume passage, apart from the single measurement that was affected by a tropospheric cloud. Following the same procedure as with the earlier figure, we find

$$\frac{\delta_{307.5}}{C_{307.5}} = 0.193 , \quad (20)$$

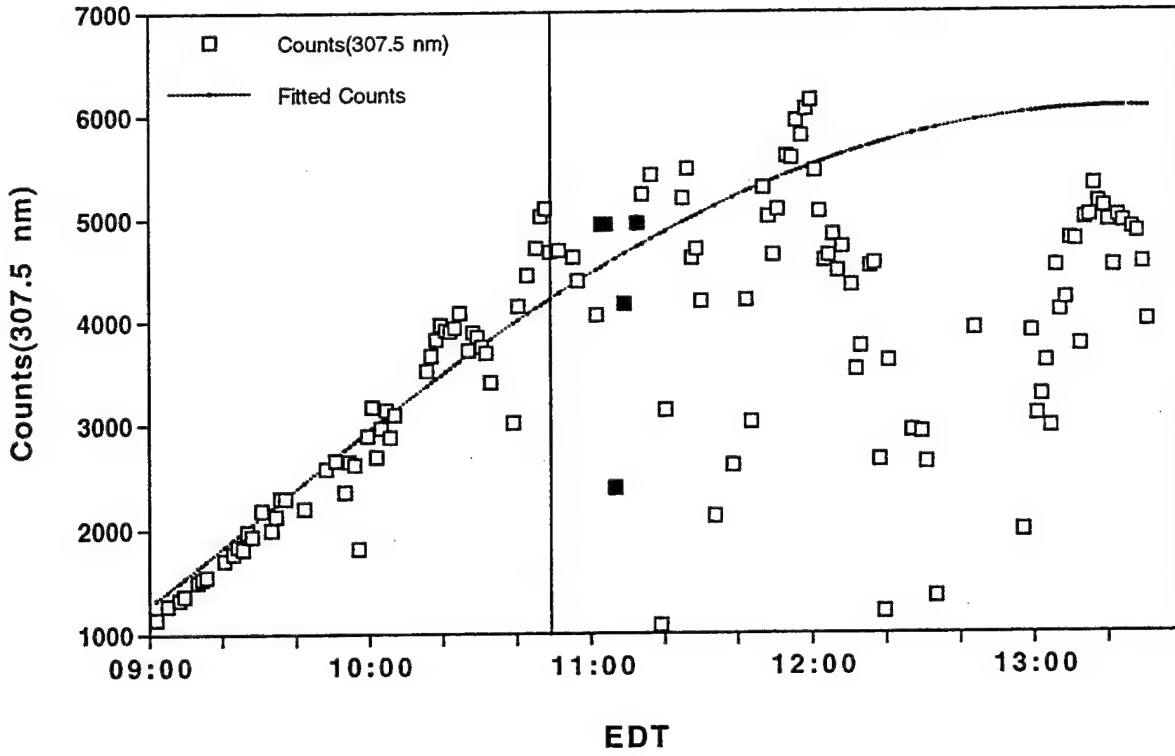


Figure 5. Similar to Figure 4 for a band centered on 307.5 nm.

and

$$\tau_R(307.5) < -\ln\left(1 - \frac{\delta_{307.5}}{\langle C_{307.5} \rangle}\right) = 0.215 \quad (21)$$

We can now demonstrate that scattering by plume particles has a negligible effect on  $R_1$  and  $R_2$ . Putting the upper limit in relation (19) into Eq. (17) gives

$$R_2 \propto \exp(\tau_{O_3}(299.0) - \tau_{O_3}(300.8)) \exp(0.167 \times 0.0243) \quad (22)$$

The last factor, which expresses the effect of plume aerosol scattering, is equal to 1.004. Therefore, Rayleigh backscattering of UV radiation by the plume has an insignificant effect on the ratios  $R_1$  and  $R_2$  from which the ozone depletion is inferred. Finally, we note that Rayleigh scattering is the worst case in terms of the wavelength sensitivity of the scattering cross-section. Therefore, any plume aerosol scattering will have a negligible effect on the derived value of total column ozone depletion.

UV spectra were also taken on June 19, the day before launch, and June 21. The June 19 data were similar to those of June 20 but covered a shorter time span and had three major interruptions of coverage. The data for  $R_1$  are plotted in Figure 6, which has the same vertical scale as Figure 2, the corresponding plot for June 20. On June 21, the observations were plagued by tropospheric clouds and finally were terminated by a sudden thunderstorm. Consequently, the plots are noisy and will not be presented here.

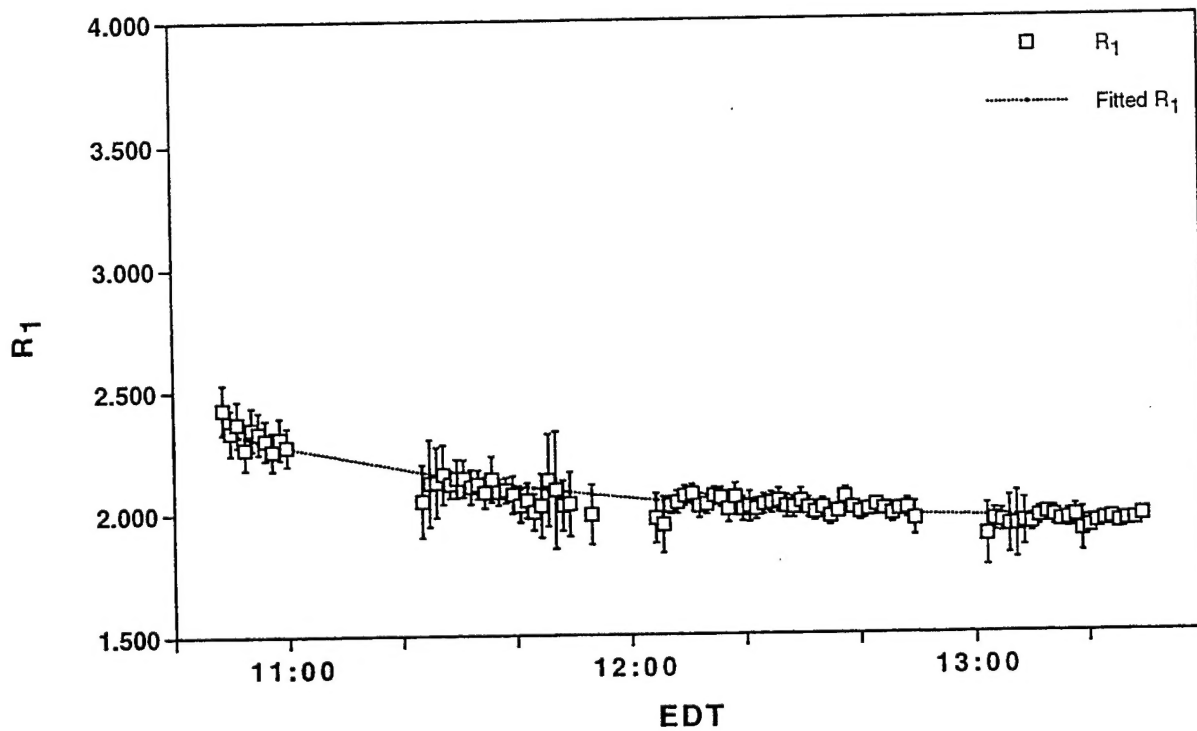


Figure 6.  $R_1$  plotted as in Figure 2 but for June 19, 1996.



#### 4. Conclusions

Following the June 20, 1996 launch of the STS-78 space shuttle mission, the stratospheric launch plume remnant was observed to drift through the line of sight from the ground-based HIROIG UV spectrograph to the sun for approximately 10 min starting 14 min after launch. The UV spectra provided no evidence of a decrease in total column ozone between the observing site and the sun during this period. From two UV intensity ratios, we derive a 95%-confidence-level upper limit on the total column ozone depletion of 3.4%, assuming a typical ambient value of 300 Dobson units. Observations of UV intensities yielded an upper limit for attenuation of radiation by scattering from plume aerosols of approximately 15% at 300.8 nm wavelength. Assuming that the aerosol scattering obeys a Rayleigh law, as suggested by earlier RISO lidar observations, such scattering has a negligible effect on the spectral ratios that are used to derive total column ozone. Since the Rayleigh law is the worst-case scattering law in terms of sensitivity of the cross section to wavelength, we can conclude that the spectral ratios were unaffected by aerosol scattering in any form.

## References

- Burke, M. L., "Monitoring of Post-Launch Ground-level UV Intensities: UNIP Results for the K-23 and STS-69 Launches," TOR-96(1410)-02 The Aerospace Corp. (5 March 1996).
- Dao, P., J. A. Gelbwachs, R. Farley, R. Garner, P. Soletsky, and G. Davidson, "LIDAR Stratospheric SRM Exhaust Plume Measurements," AIAA 35th Aerospace Sciences Meeting, Paper 97-0526 (1997).
- Denison, M. R., J. J. Lamb, W. D. Bjorndahl, E. Y. Young, and P. D. Lohn, *J. Spacecr. Rockets*, **31**, 435 (1994).
- Hackwell, J. A. and D. W. Warren, *Proc. SPIE*, **1745**, 290 (1992).
- Hecht, J., D. Gutierrez, G. Rossano, M. Sivjee, J. Skinner, D. McKenzie, and M. Ross, *Proc. SPIE*, **2266**, 352 (1994).
- Ross, M. N., *J. Spacecr. Rockets*, **33**, 435 (1996).
- Zittel, P. F., "Computer Model Calculations of the Local Effects of Large Solid Fuel Rocket Motors on Stratospheric Ozone," TR-94(4321)-19, The Aerospace Corporation, El Segundo, CA (1994).

## TECHNOLOGY OPERATIONS

The Aerospace Corporation functions as an "architect-engineer" for national security programs, specializing in advanced military space systems. The Corporation's Technology Operations supports the effective and timely development and operation of national security systems through scientific research and the application of advanced technology. Vital to the success of the Corporation is the technical staff's wide-ranging expertise and its ability to stay abreast of new technological developments and program support issues associated with rapidly evolving space systems. Contributing capabilities are provided by these individual Technology Centers:

**Electronics Technology Center:** Microelectronics, VLSI reliability, failure analysis, solid-state device physics, compound semiconductors, radiation effects, infrared and CCD detector devices, Micro-Electro-Mechanical Systems (MEMS), and data storage and display technologies; lasers and electro-optics, solid state laser design, micro-optics, optical communications, and fiber optic sensors; atomic frequency standards, applied laser spectroscopy, laser chemistry, atmospheric propagation and beam control, LIDAR/LADAR remote sensing; solar cell and array testing and evaluation, battery electrochemistry, battery testing and evaluation.

**Mechanics and Materials Technology Center:** Evaluation and characterization of new materials: metals, alloys, ceramics, polymers and composites; development and analysis of advanced materials processing and deposition techniques; nondestructive evaluation, component failure analysis and reliability; fracture mechanics and stress corrosion; analysis and evaluation of materials at cryogenic and elevated temperatures; launch vehicle fluid mechanics, heat transfer and flight dynamics; aerothermodynamics; chemical and electric propulsion; environmental chemistry; combustion processes; spacecraft structural mechanics, space environment effects on materials, hardening and vulnerability assessment; contamination, thermal and structural control; lubrication and surface phenomena; microengineering technology and microinstrument development.

**Space and Environment Technology Center:** Magnetospheric, auroral and cosmic ray physics, wave-particle interactions, magnetospheric plasma waves; atmospheric and ionospheric physics, density and composition of the upper atmosphere, remote sensing using atmospheric radiation; solar physics, infrared astronomy, infrared signature analysis; effects of solar activity, magnetic storms and nuclear explosions on the earth's atmosphere, ionosphere and magnetosphere; effects of electromagnetic and particulate radiations on space systems; space instrumentation; propellant chemistry, chemical dynamics, environmental chemistry, trace detection; atmospheric chemical reactions, atmospheric optics, light scattering, state-specific chemical reactions and radiative signatures of missile plumes, and sensor out-of-field-of-view rejection.